A Computational Investigation of the Characteristics of Velocity Slips and Convective Boundary Conditions in Maxwell Nanofluid Flow over a Permeable Stretching Surface with Activation Energy

Bidyasagar Kumbhakar[1], Manik Das[1(✉)], and Jagdev Singh[2]

[1] Department of Mathematics, National Institute of Technology Meghalaya,
Shillong 793003, India
`manikdas@nitm.ac.in`

[2] Department of Mathematics, JECRC University, Jaipur 303905, Rajasthan, India

Abstract. In this study, we analyze the effects of velocity slips and convective boundary conditions in the flow and heat transfer of Maxwell nanofluid across a stretching sheet considering magnetic field, thermal radiation, chemical reaction, and activation energy. The influence of Brownian diffusion and thermophoresis are considered using Buongiorno's nanofluid model. By applying suitable similarity variables, the governing Maxwell nanofluid flow equations, which include the momentum, energy, and nanoparticle volume fraction are simplified to nonlinear differential equations. MATLAB's *bvp4c* finite difference tool is used to solve the nondimensionalized differential equations. In order to illustrate the influence of physical factors on velocity, temperature, and nanoparticle volume fraction, the numerical solutions are shown graphically. In addition, the skin friction, rate of heat transmission, and mass transfer are all given physical interpretations. The current analysis demonstrates that the velocity slip and suction parameters significantly reduce the velocity. Increased thermal radiation and Biot number for temperature raise the temperature profile. Further, the activation energy and thermophoresis factors lead to a decrease in the mass transfer rate, while the Lewis number and Biot number due to concentration contribute to an increase.

Keywords: Hall effect · Radiation absorption · Thermal radiation · Chemical reaction · Convective heating · Activation energy

Nomenclature

T	Temperature	K_1	Chemical reaction parameter
c	Velocity ratio parameter	h_2	Convective mass transfer coefficient
u, v, w	Velocity components	k_r^2	Chemical reaction coefficient
M	Magnetic parameter	B_0	Constant magnetic field
x, y, z	Space coordinates	D_T	Coefficient of thermal diffusion
K	Deborah number	Bi_1	Biot number for temperature
n	Fitted rate constant	Bi_2	Biot number for concentration
Le	Lewis number	w_0	Suction velocity
$u_\mathrm{w}, v_\mathrm{w}$	Stretching velocities	**Greek Symbols**	
E	Dimensionless activation energy	α_1	Velocity slip parameter
k	Thermal conductivity	μ	Dynamic viscosity
k^*	Mean absorption coefficient	θ_w	Temperature ratio parameter
T_∞, C_∞	Ambient temperature and concentration	κ	Boltzmann constant
S	Suction parameter	ρ	Density
Rd	Thermal radiation parameter	θ	Dimensionless temperature
Pr	Prandtl number	λ	Fluid relaxation time
c_p	Specific heat	α	Thermal diffusivity
C	Concentration	ν	Kinematic viscosity
Nt	Thermophoresis parameter	ϕ	Dimensionless concentration
$T_\mathrm{w}, C_\mathrm{w}$	Surface temperature and concentration	σ^*	Stefan-Boltzmann constant
Nb	Brownian motion parameter	β	Slip coefficient
E_a	Activation energy	σ	Electrical conductivity
D_B	Mass diffusivity	τ	Ratio between effective heat capacity
h_1	Convective heat transfer coefficient		of nanoparticles and base fluid

1   Introduction

In the petroleum industry and engineering applications, non-Newtonian fluid flow coupled with heat and mass transfer is of significant interest. Desalination, refrigeration and air conditioning, compact heat exchangers, chemical processing equipment, solid matrix heat exchangers, solar power collectors, and other applications [1,2] are examples. The Laplace and Hankel transforms were used to calculate the velocity field and shear stress field of a generalised Maxwell fluid that flows between two infinite coaxial circular cylinders [3]. By employing the multi-step differential transform approach, Keimanesh et al. [4] investigated third grade non-Newtonian fluid flow between two parallel plates. Nadeem et al. [5] presented a model of a two-dimensional Williamson fluid past a stretched sheet that they had developed. Seyedi et al. [6] investigated effect of natural convection on non-Newtonian fluid flow between two vertical plates using Galerkin interpolation scaling functions.

Thermal radiation effects on nanofluid flow and heat transfer are becoming increasingly popular because nanofluids have a variety of characteristics. In addition, the influence of radiative heat transfer has increased dramatically in the design of modern energy conversion systems [7], plasma studies, agriculture, and petroleum industries [8,9]. Numerous research have been conducted in this area to investigate the impacts of heat radiation in various areas. A two-dimensional MHD mixed convection viscoelastic fluid flow across a porous wedge with heat radiation was investigated by Rashidi et al. [10], who sought an analytical solution. Daniel and Daniel [11] did research on the theoretical impact of buoyancy and heat radiation on MHD flow past a stretched porous sheet. Pal and Mandal [12] discussed the influence of thermal radiation, non-uniform heat source/sink and suction on MHD micropolar nanofluid flow across a stretched sheet. MHD viscous fluid was flowed over a horizontally rotating disc, and Shah et al. [13] explored the effect of non-linear thermal radiations on the unsteady flow of the fluid. Effect of thermal radiation on MHD stagnation-point flow over a nonlinearly moving sheet was described by Jamaludin et al. [14] with mathematical solutions. Tarakaramu et al. [15] investigated the impact of nonlinear thermal radiation and Joule heating on the flow of a three-dimensional viscoelastic nanofluid via a stretched surface.

In various physical scenarios involving suspensions, foams and polymer solutions [16], the assumption of slip flow boundary condition is necessary. The no-slip boundary condition is involved in the research listed above. With the Soret and Dufoue effect, Babu and Sandeep [17] investigated multiple slip effects on the magnetohydrodynamic Williamson fluid flow past a variable thickness stretching sheet. Using a non-isothermal radiate wedge submerged in ferrofluid, Rashad [18] analysed the impact of partial slip and thermal radiation on MHD boundary layer flow in his research. With entropy analysis, Ellahi et al. [19] looked at the combined impact of MHD and slip on a flat moving plate over a wide range of physical factors. Das et al. [20] examined multiple slips as well as nonlinearly changing thermal radiation on a 3D MHD nonlinear convective tangent hyperbolic nanofluid flow generated by a bidirectional stretching surface with Soret and Dufour impacts.

In the investigation of a number of physical phenomena, including engineering and oil storage, activation energy is often taken into consideration. A few theoretical studies that discuss the function of activation energy in fluid dynamics are currently available. Numerous uses of Arrhenius activation energy, as well as chemical reactions, have made fluid dynamics an appealing area for researchers. The least amount of energy required to stimulate the particles or molecules in which physical transit occurs is known as activation energy. This is due to the fact that different chemical processes need some amount of energy merely to begin. Other uses of activation energy include atomic processes, the discovery of compounds, and thermal lubricant recovery [21–23]. Fayyadh et al. [24] investigated the magneto-flow and heat transfer of the Carreau nanofluids model in the presence of Arrhenius activation energy and chemical reaction toward a stretching/shrinking surface. Akbar et al. [25] studied the effects of gyrotactic motile

microorganisms and Arrhenius activation on the bioconvection peristaltic transport of nanofluid. They also considered variable viscosity, Brownian diffusion, porous medium, mixed convection, nonuniform heat absorption/generation, viscous dissipation, and thermophoresis diffusion. Shoaib et al. [26] examined the significance of activation energy during chemical reactions, temperature gradient, and thermal radiations of 3-D steady magnetite Casson nanofluid flow over an oscillating disk.

Convective heating is very common in engineering practises such as nuclear reactors, gas turbines and thermal energy storage [27, 28]. These activities generate a high temperature, which is transferred to the flow via the convective boundary condition. To better understand the impact of convective boundary conditions on the MHD flow of nanofluids near a stretching rotaing disc with partial slip effects, Mustafa and Khan [29] carried out a numerical study. On mixed convection MHD micropolar fluid with non-linear stretched sheet, Patel and Singh [30] investigated the impacts of convective heat boundary condition, viscous dissipation and Joule heating, among other things. MHD Casson fluid flow across an exponentially extending curved sheet was studied by Kumar et al. [31] and shown to be affected by convective heating, thermal radiation and Joule heating. Das et al. [32] explored effects of convective heating, velocity slips, and activation energy on unsteady MHD 3D Carreau nanofluid flow over a stretching sheet. Mandal et al. [33] examined the convective heat transfer and entropy generation of magnetohydrodynamic Maxwell nanofluid flow including gyrotactic microorganisms along a stretching cylinder with heat source and chemical reaction.

To the best of the authors' knowledge, no studies have reported the impacts of velocity slip, activation energy, and convective heating on Maxwell nanofluid to this day. Hence, the purpose of this study is to investigate the effects of velocity slip, activation energy, and convective heating on MHD Maxwell nanofluid flow via a permeable stretching surface when thermal radiation is present. The problem of non Newtonian nanofluid flow across a stretched surface is extremely helpful in gas turbines, aerodynamic heating, food processes, biomedicines, polymer processing, and other fields. In order to convert the dimensional governing equations into their dimensionless counterparts, proper similarity transformations have been used. The *bvp4c* solver in MATLAB is applied to simulate reduced highly nonlinear ordinary differential equations. The effects of significant factors on the momentum, temperature, concentration, and skin friction coefficients, as well as the Nusselt and Sherwood numbers, are graphically depicted.
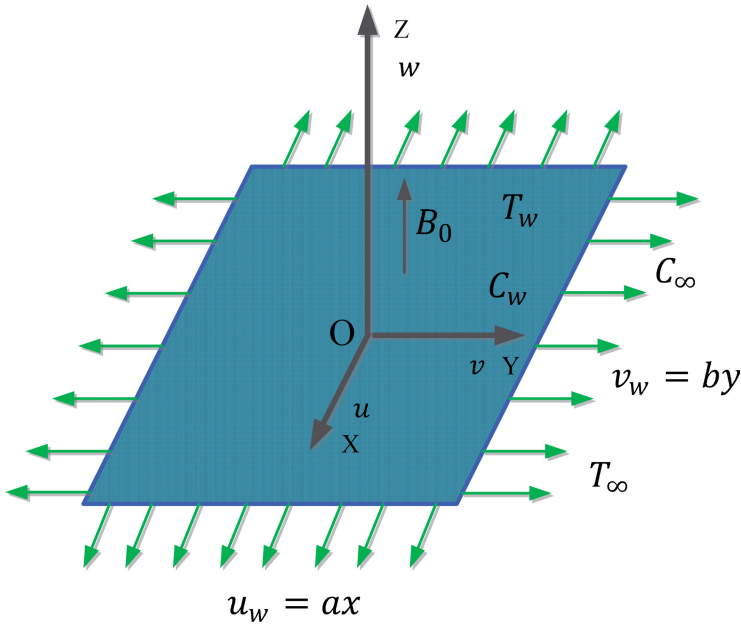
2   Mathematical Modelling

Fig. 1. Geometry of the flow problem

Consider a 3D Maxwell nanofluid flow across a stretched surface in the xy-plane, with the fluid at $z \geq 0$. In the x-direction, the sheet is stretched with a linear velocities of $u_w = ax$ and $v_w = by$ (a and b being positive constants). We'll call these two values T_w and C_w, the surface temperatures and concentrations. T_∞ and C_∞, on the other hand, represent the temperature and concentration far away from the surface, as illustrated in Fig. 1. The stretched surface is subjected to a magnetic force of strength B_0, which is applied normal to the surface. Thermal radiation and activation energy are considered to study the fluid flow. Another consideration is that the flow field does not have any polarization of charges since no external electric field is applied, which corresponds to the condition when no energy is injected or withdrawn from the fluid by electrical methods. Furthermore, a fluid with a low magnetic Reynolds number is thought to be a metallic liquid or partly ionized. So fluid motion's effect on the induced magnetic field is minuscule in compared to the applied magnetic field. The governing equations may be reconstructed on the basis of the aforementioned flow assumptions [34,35]:

$$\frac{\partial u}{\partial x} + \frac{\partial v}{\partial y} + \frac{\partial w}{\partial z} = 0, \tag{1}$$

$$u\frac{\partial u}{\partial x} + v\frac{\partial u}{\partial y} + w\frac{\partial u}{\partial z} + \lambda\left(u^2\frac{\partial^2 u}{\partial x^2} + v^2\frac{\partial^2 u}{\partial y^2} + 2uv\frac{\partial^2 u}{\partial x\partial y} + 2uw\frac{\partial^2 u}{\partial x\partial z} + 2vw\frac{\partial^2 u}{\partial y\partial z}\right)$$
$$= \nu\frac{\partial^2 u}{\partial z^2} - \frac{\sigma B_0^2}{\rho_f}\left(u + \lambda w\frac{\partial u}{\partial z}\right), \tag{2}$$

$$u\frac{\partial v}{\partial x} + v\frac{\partial v}{\partial y} + w\frac{\partial v}{\partial z} + \lambda\left(u^2\frac{\partial^2 v}{\partial x^2} + v^2\frac{\partial^2 v}{\partial y^2} + 2uv\frac{\partial^2 v}{\partial x\partial y} + 2vw\frac{\partial^2 v}{\partial y\partial z} + 2uw\frac{\partial^2 v}{\partial x\partial z}\right)$$
$$= \nu\frac{\partial^2 v}{\partial z^2} - \frac{\sigma B_0^2}{\rho_f}\left(v + \lambda w\frac{\partial v}{\partial z}\right), \tag{3}$$

$$u\frac{\partial T}{\partial x} + v\frac{\partial T}{\partial y} + w\frac{\partial T}{\partial z} = \alpha\frac{\partial^2 T}{\partial z^2} + \tau\left\{D_B\frac{\partial T}{\partial z}\frac{\partial C}{\partial z} + \frac{D_T}{T_\infty}\left(\frac{\partial T}{\partial z}\right)^2\right\} - \frac{1}{(\rho c_p)_f}\frac{\partial q_r}{\partial z}, \tag{4}$$

$$u\frac{\partial C}{\partial x} + v\frac{\partial C}{\partial y} + w\frac{\partial C}{\partial z} = D_B\frac{\partial^2 C}{\partial z^2} + \frac{D_T}{T_\infty}\frac{\partial^2 T}{\partial z^2} - k_r^2(C - C_\infty)\left(\frac{T}{T_\infty}\right)^n e^{\left(\frac{-E_a}{\kappa T}\right)}. \tag{5}$$

The following are the physical boundary conditions for the present problem [36–38]:

$$u - ax + \lambda\left(u\frac{\partial u}{\partial x} - au + v\frac{\partial u}{\partial y} + w\frac{\partial u}{\partial z}\right) = \beta\frac{\partial u}{\partial z}, \quad v - by + \lambda\left(u\frac{\partial v}{\partial x} - bv + v\frac{\partial v}{\partial y} + w\frac{\partial v}{\partial z}\right) = \beta\frac{\partial v}{\partial z}, \quad w = w_0,$$
$$-k\frac{\partial T}{\partial z} = h_1(T_w - T), \quad -D_B\frac{\partial C}{\partial z} = h_2(C_w - C), \quad \text{at } z = 0,$$
$$u \to 0, \quad v \to 0, \quad T \to T_\infty, \quad C \to C_\infty \quad \text{as} \quad z \to \infty. \tag{6}$$

The following Rosseland's estimate for an optically thick fluid is used to approximate the radiative heat flux q_r [39]:

$$q_r = -\frac{16\sigma^* T^3}{3k^*}\frac{\partial T}{\partial z}. \tag{7}$$

The energy equation has the following form when expression (7) is applied to Eq. (4):

$$u\frac{\partial T}{\partial x} + v\frac{\partial T}{\partial y} + w\frac{\partial T}{\partial z} = \alpha\frac{\partial^2 T}{\partial z^2} + \tau\left\{D_B\frac{\partial T}{\partial z}\frac{\partial C}{\partial z} + \frac{D_T}{T_\infty}\left(\frac{\partial T}{\partial z}\right)^2\right\} + \frac{16\sigma^* T^2}{(3\rho c_p)_f k^*}\left\{T\frac{\partial^2 T}{\partial Z^2} + 3\left(\frac{\partial T}{\partial Z}\right)^2\right\}. \tag{8}$$

The following similarity variables are included in order to achieve similar solutions for Eqs. (2), (3), (8), and (5), subject to the boundary constraints (6):

$$u = axf'(\eta), \quad v = ayg(\eta), \quad w = -\sqrt{a\nu}(f(\eta) + g(\eta)), \quad \theta(\eta) = \frac{T - T_\infty}{T_w - T_\infty}, \quad \phi(\eta) = \frac{C - C_\infty}{C_w - C_\infty}, \quad \eta = z\sqrt{\frac{a}{\nu}}. \tag{9}$$

The following ordinary differential equations result from substituting the aforementioned similarity variables in Eqs. (2), (3), (8), and (5):

$$f''' - f'^2 + (MK + 1)(f + g)f'' + K(2f'(f + g)f'' - (f + g)^2 f''') - Mf' = 0, \tag{10}$$

$$g''' - g'^2 + (MK + 1)(f + g)g'' + K(2g'(f + g)g'' - (f + g)^2 g''') - Mg' = 0, \tag{11}$$

$$\theta'' + Pr(f + g)\theta' + PrNb\theta'\phi' + PrNt\left(\theta'\right)^2 + \frac{4}{3}Rd\left\{1 + \theta\left(\theta_\mathrm{w} - 1\right)\right\}^2 \left[3\left(\theta'\right)^2(\theta_\mathrm{w} - 1)\right.$$
$$\left. + \left\{1 + \theta\left(\theta_\mathrm{w} - 1\right)\right\}\theta''\right] = 0, \tag{12}$$

$$\phi'' + PrLe(f + g)\phi' + \frac{Nt}{Nb}\theta'' - PrLeK_1(1 + (\theta_\mathrm{w} - 1)\theta)^n e^{\left(-\frac{E}{1 + (\theta_\mathrm{w} - 1)\theta}\right)}\phi = 0. \tag{13}$$

The dimensionless boundary conditions are written as follows:

$$\left.\begin{array}{l} f'(0) = 1 - K\left\{f'^2 - f' - (f + g)f''\right\} + \alpha_1 f'', \quad g'(0) = c - K\left\{g'^2 - cg' - (f + g)g''\right\} + \alpha_1 g'', \\[2mm] f(0) = S, \quad g(0) = 0, \quad \theta'(0) = -Bi_1\left(1 - \theta(0)\right), \quad \phi'(0) = -Bi_2\left(1 - \phi(0)\right), \\[2mm] f'(\infty) \to 0, \quad g(\infty) \to 0, \quad \theta(\infty) \to 0, \quad \phi(\infty) \to 0. \end{array}\right\} \tag{14}$$

where

$$K = \lambda a, \quad Pr = \frac{\nu}{\alpha}, \quad M = \frac{\sigma B_0^2}{a\rho_f}, \quad Nb = \frac{\tau D_B(C_\mathrm{w} - C_\infty)}{\nu}, \quad Nt =$$
$$\frac{\tau D_T(T_\mathrm{w} - T_\infty)}{\nu T_\infty}, \quad \alpha_1 = \beta\sqrt{\frac{a}{\nu}}, \quad S = -\frac{w_0}{\sqrt{a\nu}}, \quad K_1 = \frac{k_r^2}{a}, \quad \theta_\mathrm{w} = \frac{T_\mathrm{w}}{T_\infty}, \quad E = \frac{E_a}{\kappa T_\infty},$$
$$Bi_1 = \frac{h_1}{k}\sqrt{\frac{\nu}{a}}, \quad Rd = \frac{4\sigma^* T_\infty^3}{k^* k}, \quad c = \frac{b}{a}, \quad Le = \frac{\alpha}{D_B}, \quad Bi_2 = \frac{h_2}{D_B}\sqrt{\frac{\nu}{a}}.$$

3   Local Skin-Friction Coefficients, Nusselt Number and Sherwood Number

In this fluid flow problem, the local skin-friction coefficients (C_{fx}, C_{fy}), Nusselt number (Nu_x), and Sherwood number (Sh_x) are the relevant physical quantities, and their expressions are as follows:

$$C_{fx} = \frac{\nu}{u_\mathrm{w}^2}\left[(1 + K)\frac{\partial u}{\partial z}\right]_{z=0}, \tag{15}$$

$$C_{fy} = \frac{\nu}{v_\mathrm{w}^2}\left[(1 + K)\frac{\partial v}{\partial z}\right]_{z=0}, \tag{16}$$

$$Nu_x = -\frac{x}{k(T_\mathrm{w} - T_\infty)}\left[\left(k + \frac{16\sigma^* T^3}{3k^*}\right)\frac{\partial T}{\partial z}\right]_{z=0}, \tag{17}$$

$$Sh_x = -\frac{xD_B}{D_B(C_\mathrm{w} - C_\infty)}\left(\frac{\partial C}{\partial z}\right)_{z=0}. \tag{18}$$

Using the dimensionless variables provided in (9), the aforementioned physical quantities may be stated in non-dimensional form

$$C_{fx}\sqrt{Re_x} = (1 + K)f''(0), \tag{19}$$

$$C_{fy}\sqrt{Re_y} = (c)^{-\frac{3}{2}}(1 + K)g''(0), \tag{20}$$

$$\frac{Nu_x}{\sqrt{Re_x}} = -\left[1 + \frac{4}{3}Rd\left\{1 + (\theta_\mathrm{w} - 1)\theta(0)\right\}^3\right]\theta'(0), \tag{21}$$

$$\frac{Sh_x}{\sqrt{Re_x}} = -\phi'(0), \tag{22}$$

where $Re_x = \dfrac{u_{\mathrm{w}}x}{\nu}$ and $Re_y = \dfrac{v_{\mathrm{w}}y}{\nu}$ are the local Reynolds numbers.

4   Implementation of Numerical Technique

4.1   Solution Procedure

MATLAB's bvp4c code is used to solve the nonlinear ordinary differential equations (ODE) that govern flow Eqs. (10–13) with boundary conditions 14. Other researchers have extensively implemented this code to tackle the boundary value issue. The MATLAB routine is a representation of a finite difference algorithm that achieves fourth-order precision. For the solver to work, the equations need to be rewritten as a system of equivalent first-order differential equations.

4.2   Results Validation

To validate the employed technique, we got $-f''(0)$ and $-g''(0)$ values and compared them to earlier reported results by Hayat and Awais [40] and Kumar et al. [8] in Tables 1 and 2 where $M = K = \alpha_1 = S = 0.0$ for a variety of c values. It is recognized that the comparison is realistic, which provides assurance of the accuracy of the numerical results presented in this study.

Table 1. Comparison of $-f''(0)$'s numerical findings with previously published data

c	$-f''(0)$		
	Hayat and Awais [40]	Kumar et al. [8]	Present result
0	1	1.000003	1
0.2	1.039495	1.039498	1.039498
0.4	1.075788	1.075789	1.075789
0.6	1.109946	1.109948	1.109947
0.8	1.142488	1.142490	1.142488
1.0	1.173720	1.173722	1.173720

Table 2. Comparison of $-g''(0)$'s numerical findings with previously published data

c	$-g''(0)$		
	Hayat and Awais [40]	Kumar et al. [8]	Present result
0	0	0	0
0.2	0.148736	0.148738	0.148738
0.4	0.349208	0.349209	0.349210
0.6	0.590528	0.590526	0.590529
0.8	0.866682	0.866679	0.866683
1.0	1.173720	1.173717	1.173720
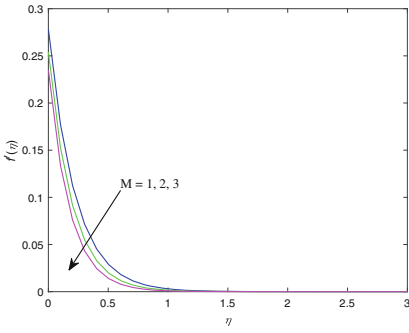
Fig. 2. Impact of M on $f'(\eta)$
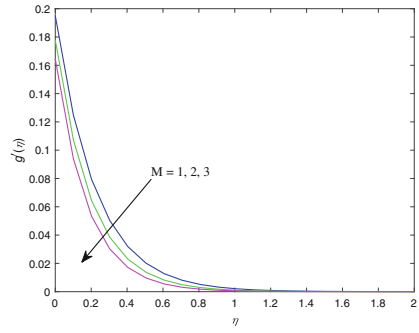
Fig. 3. Impact of M on $g'(\eta)$

5   Results and Discussion

Many important factors have been looked at in this section. They have an effect on velocities, temperature, concentration, skin friction, rate of heat transfer, and rate of mass transfer. To do the calculations, we chose $K = 0.1$, $Pr = S = 2.0$, $Nt = n = 0.5$, $M = 1$, $Rd = K_1 = 0.2$, $Nb = \alpha_1 = 0.4$, $Le = 1$, $\theta_w = 1.3$, $Bi_1 = Bi_2 = 0.3$, $E = 0.6$ and $c = 0.7$.

Figures 2 and 3 demonstrate the non-dimensional velocities $f'(\eta)$ and $g'(\eta)$ for different magnetic field parameter values M. The velocities $f'(\eta)$ and $g'(\eta)$ decrease as the magnetic parameter M increases. The physical explanation for this behavior is that increasing the magnetic parameter operating transverse to the flow enhances the Lorentz force, which tends to resist the fluid motion. The velocity slip parameter α_1 has a significant impact on fluid flow, as seen in Figs. 4 and 5. By raising the velocity parameter α_1, the velocities $f'(\eta)$ and $g'(\eta)$ decrease. The slip between the fluid and the sheet surface increases as the velocity slip parameters rise. As a result, a partial slip velocity is transferred to the flow-field that tends to minimize fluid velocities. Figures 6 and 7 express that enhanced values of S imply the decreasing nature of flow velocities. Suction is
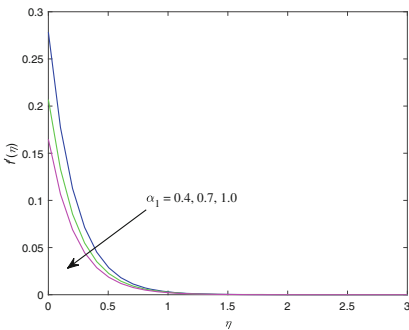
Fig. 4. Impact of α_1 on $f'(\eta)$
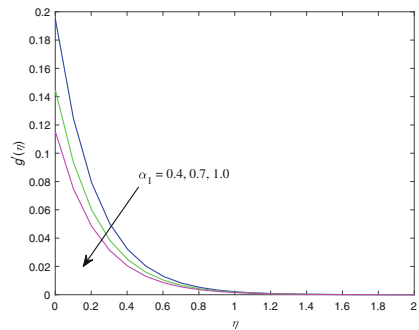
Fig. 5. Impact of α_1 on $g'(\eta)$
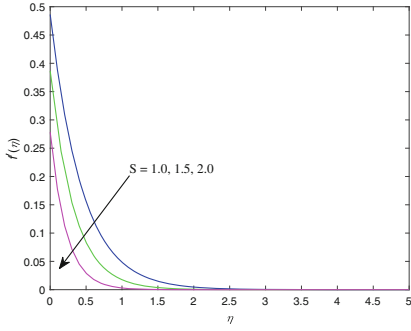
Fig. 6. Impact of S on $f'(\eta)$
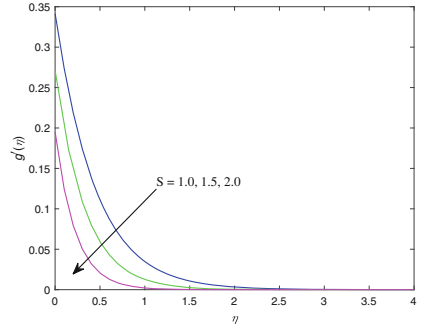
Fig. 7. Impact of S on $g'(\eta)$
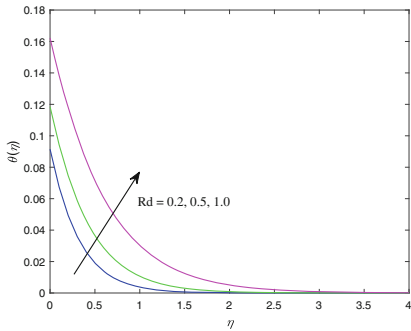

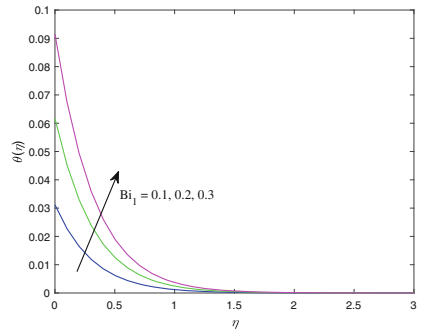**Fig. 8.** Impact of Rd on $\theta(\eta)$

Fig. 9. Impact of Bi_1 on $\theta(\eta)$
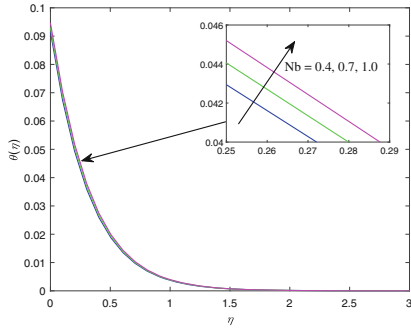

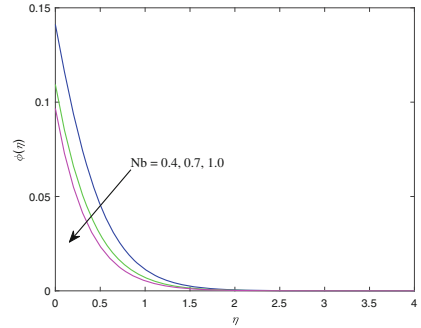**Fig. 10.** Impact of Nb on $\theta(\eta)$

Fig. 11. Impact of Nb on $\phi(\eta)$

utilized to regulate the nanofluid flow physically, with the purpose of reducing velocities by minimizing drag on nanoparticles in an external flow.

Figure 8 illustrates the effect of the thermal radiation parameter Rd on the temperature distribution. The graphic clearly shows that with increasing Rd values, $\theta(\eta)$ is upsurged. In general, increasing radiative characteristics promote
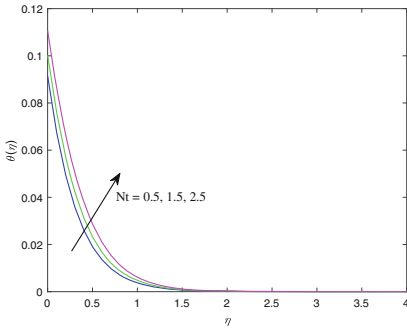
Fig. 12. Impact of Nt on $\theta(\eta)$
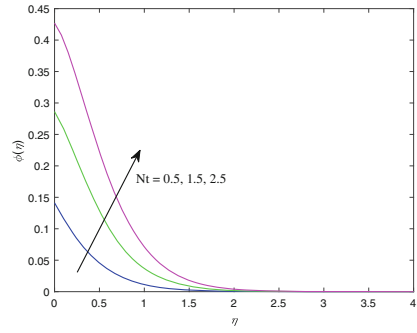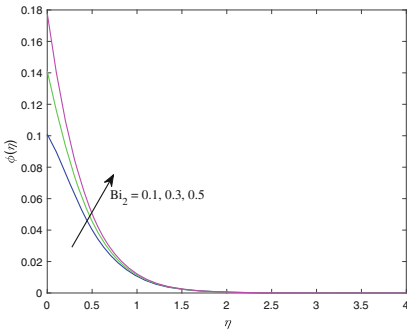

Fig. 13. Impact of Nt on $\phi(\eta)$

Fig. 14. Impact of Bi_2 on $\phi(\eta)$
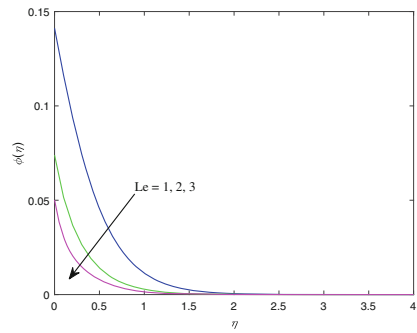

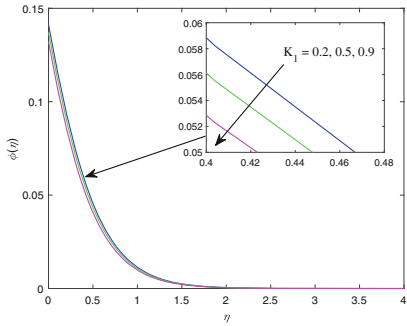**Fig. 15.** Impact of Le on $\phi(\eta)$

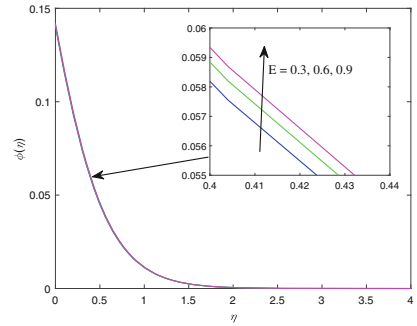**Fig. 16.** Impact of K_1 on $\phi(\eta)$

Fig. 17. Impact of E on $\phi(\eta)$

molecular mobility within the system, resulting in frequent collisions between particles that convert to heat energy. As a result, the temperature has risen. The effect of Biot number for temeperature on the temperature field is explored in Fig. 9. The increase in Bi_1 indicates that conduction dominates convection heat transfer at the surface. Consequently, for higher Bi_1 values, temperature
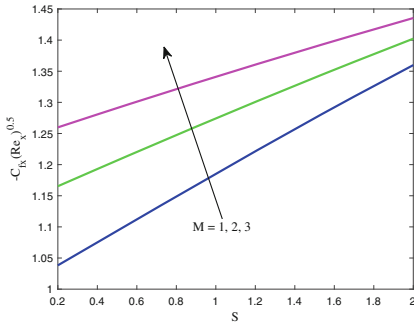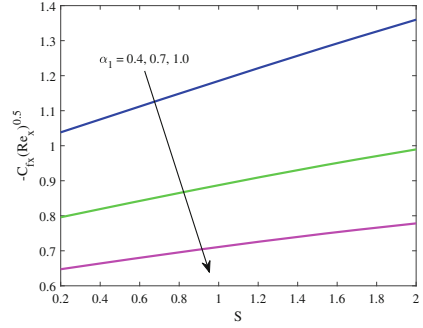
Fig. 18. Impact of M and S on $-C_{fx}\sqrt{Re_x}$

Fig. 19. Impact of α_1 and S on $-C_{fx}\sqrt{Re_x}$
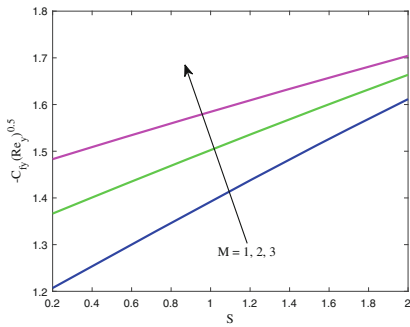
Fig. 20. Impact of M and S on $-C_{fy}\sqrt{Re_y}$
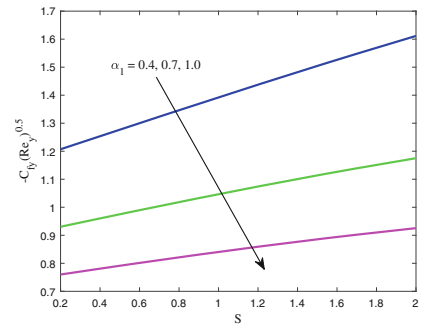

Fig. 21. Impact of α_1 and S on $-C_{fy}\sqrt{Re_y}$

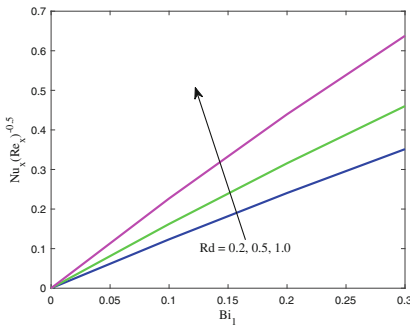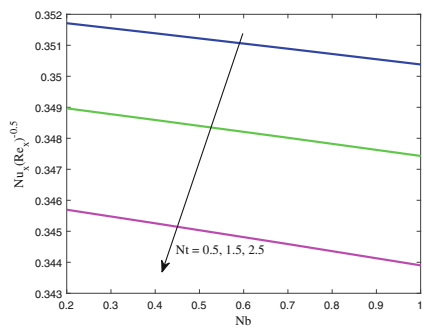**Fig. 22.** Impact of Rd and Bi_1 on $\frac{Nu_x}{\sqrt{Re_x}}$

Fig. 23. Impact of Nt and Nb on $\frac{Nu_x}{\sqrt{Re_x}}$

curves are accelerated. According to Figs. 10 and 11, an increase in Nb results in an increase in $\theta(\eta)$ and a decrease in $\phi(\eta)$ over the boundary layer area. When microscopic particles in the flow field come into contact with one other, they
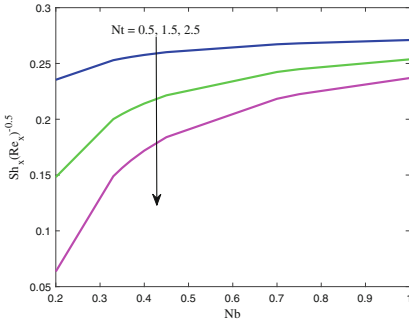
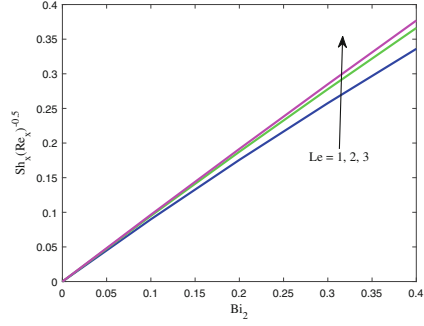**Fig. 24.** Impact of Nt and Nb on $\frac{Sh_x}{\sqrt{Re_x}}$

Fig. 25. Impact of Le and Bi_2 on $\frac{Sh_x}{\sqrt{Re_x}}$

create thermal energy, raising the fluid temperature. As a result of Brownian diffusion, the volume fraction of nanoparticles in the boundary layer decreases as they recede from the sheet's surface. It is clear from Figs. 12 and 13 that when Nt grows, $\theta(\eta)$ and $\phi(\eta)$ rise with it. When a nanoparticle in touch with a stretched sheet is heated by the sheet's temperature, it exhibits a thermophoretic force that causes it to push back other nanoparticles in its vicinity. An increase in Nt raises the thermophoretic force, which drives the nanoparticles from a hot location to a cool one inside the boundary layer, increasing he temperature of the nanofluid and the volume fraction of the nanoparticles. Figure 14 shows the influence of Bi_2 on the dispersion of concentration. The graphic demonstrates that there is a direct relationship between $\phi(\eta)$ and Bi_2. As the Brownian diffusivity coefficient is inversely proportional to the Bi_2, this means the velocity-dependent diffusion of momentum is more powerful than the temperature-dependent diffusion. So, $\phi(\eta)$ is amplified. Figure 15 depicts the relationship between the Lewis number Le and the concentration profile. $\phi(\eta)$ decelerates as Le increases throughout the boundary layer area. The Lewis number is the ratio of heat diffusivity to mass diffusivity, according to its definition. Increasing the Lewis number means that there is more thermal diffusion and less mass diffusion, which makes the concentration boundary layer thinner. The influence of the chemical reaction parameter K_1 on species concentration is depicted in Fig. 16. We can observe from this graph that as K_1 increases, $\phi(\eta)$ falls. This is because there is more thermal energy available to obtain the activation energy required to compensate for the breakdown of atoms' bonds. The activation energy parameter E has been displayed in Fig. 17 to show how it affects concentration distribution. This diagram clearly shows that $\phi(\eta)$ and E have a direct relationship. As E increases, the pace of a chemical reaction physically increases. Hence, $\phi(\eta)$ is heightened.

The differences in the local surface drag coefficients $-C_{fx}\sqrt{Re_x}$ and $-C_{fy}\sqrt{Re_y}$ scatterings of Maxwell nanofluid as a function of M, α_1, and S are depicted in Figs. 18, 19, 20 and 21. The figures demonstrate that $-C_{fx}\sqrt{Re_x}$ and $-C_{fy}\sqrt{Re_y}$ degrade with increasing α_1 values, but M and S exhibit the opposite pattern. Figures 22 and 23 illustrate the effects of Rd, Bi_1, Nt and
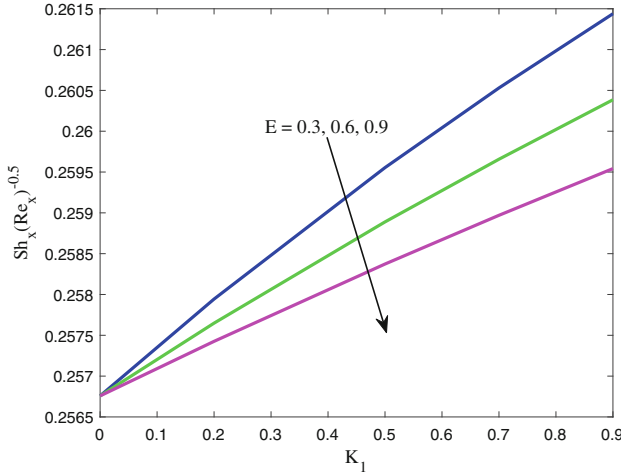
Fig. 26. Impact of E and K_1 on $\frac{Sh_x}{\sqrt{Re_x}}$

Nb on the local Nusselt number $\frac{Nu_x}{\sqrt{Re_x}}$. On the basis of the figures, it can be concluded that $\frac{Nu_x}{\sqrt{Re_x}}$ is directly proportional to Rd and Bi_1, however an inverse relationship can be noticed between Nt and Nb. The effects of Nt, Nb, Le, Bi_2, K_1, and E on local mass transfer rate $\frac{Sh_x}{\sqrt{Re_x}}$ scattering are displayed in Figs. 24, 25 and 26. Figures show that $\frac{Sh_x}{\sqrt{Re_x}}$ is heightened with increasing amounts of Nb, Le, Bi_2, and K_1, whereas an inverse association is noticed with Nt and E.

6   Conclusions

The effects of velocity slip, activation energy, and convective heating on MHD Maxwell nanofluid flow across a permeable stretched surface heated by thermal radiation are examined computationally in this study using MATLAB's *bvp4c* solver. The following conclusions are made from the findings:

– For increasing levels of the velocity slip and suction parameters, the velocity decreases in magnitude.
– Increasing the Biot number for temperature and thermal radiation can enhance temperature profiles.
– Concentration field increases with an elevation in the Biot number for concentration and the activation energy parameter.
– Increases in the magnetic field and suction parameter augment the shear stress function, whilst velocity slip lowers it.
– The combination of radiation absorption, thermal radiation, and convection heating can all help to boost the heat transmission rate.
– Activation energy can uplift mass transfer rate while chemical reaction slows it down.

References

1. Dogonchi, A.S., Ganji, D.D.: Investigation of heat transfer for cooling turbine disks with a non-Newtonian fluid flow using DRA. Case Stud. Therm. Eng. **6**, 40–51 (2015)
2. Rashidi, M.M., Bagheri, S., Momoniat, E., Freidoonimehr, N.: Entropy analysis of convective MHD flow of third grade non-Newtonian fluid over a stretching sheet. Ain Shams Eng. J. **8**(1), 77–85 (2017)
3. Mahmood, A., Parveen, S., Ara, A., Khan, N.A.: Exact analytic solutions for the unsteady flow of a non-Newtonian fluid between two cylinders with fractional derivative model. Commun. Nonlinear Sci. Numer. Simul. **14**, 3309–3319 (2009)
4. Keimanesh, M., Rashidi, M.M., Chamkha, A.J., Jafari, R.: Study of a third grade non-newtonian fluid flow between two parallel plates using the multi-step differential transform method. Comput. Math. Appl. **62**(8), 2871–2891 (2011)
5. Nadeem, S., Hussain, S.T., Lee, C.: Flow of a Williamson fluid over a stretching sheet. Braz. J. Chem. Eng. **30**(3), 619–625 (2013)
6. Seyedi, S.H., Saray, B.N., Nobari, M.R.H.: Using interpolation scaling functions based on Galerkin method for solving non-Newtonian fluid flow between two vertical at plates. Appl. Math. Comput. **269**, 488–496 (2015)
7. Nandi, S., Kumbhakar, B.: Hall current and thermo-diffusion effects on magneto-hydrodynamic convective flow near an oscillatory plate with ramped type thermal and solutal boundary conditions. Indian J. Phys. **96**, 763–776 (2022)
8. Kumar, S.G., Varma, S.V.K., Prasad, P.D., Raju, C.S.K., Makinde, O.D., Sharma, R.: MHD reacting and radiating 3-D flow of Maxwell fluid past a stretching sheet with heat source/sink and Soret effects in a porous Medium. Defect Diffus. Forum **384**, 145–156 (2018)
9. Makinde, O.D., Mabood, F., Ibrahim, M.S.: Chemically reacting on MHD boundary-layer flow of nanofluids over a non-linear stretching sheet with heat source/sink and thermal radiation. Therm. Sci. **22**(1), 495–506 (2018)
10. Rashidi, M.M., Ali, M., Freidoonimehr, N., Rostami, B., Hossain, M.A.: Mixed convective heat transfer for MHD viscoelastic fluid flow over a porous wedge with thermal radiation. Adv. Mech. Eng. **2014**, 735939 (2014)
11. Daniel, Y.S., Daniel, S.K.: Effects of buoyancy and thermal radiation on MHD flow over a stretching porous sheet using homotopy analysis method. Alex. Eng. J. **54**(3), 705–712 (2015)
12. Pal, D., Mandal, G.: Thermal radiation and MHD effects on boundary layer flow of micropolar nanofluid past a stretching sheet with non-uniform heat source/sink. Int. J. Mech. Sci. **126**, 307–318 (2017)
13. Shah, Z., Dawar, A., Kumam, P., Khan, W., Islam, S.: Impact of nonlinear thermal radiation on MHD nanofluid thinfilm flow over a horizontally rotating disk. Appl. Sci. **9**(8), 1533 (2019)
14. Jamaludin, A., Naganthran, K., Nazar, R., Pop, I.: Thermal radiation and MHD effects in the mixed convection flow of Fe_3O_4-Water ferrofluid towards a nonlinearly moving surface. Processes **8**(1), 95 (2020)
15. Tarakaramu, N., Narayana, P.V.S., Babu, D.H., Sarojamma, G., Makinde, O.D.: Joule heating and dissipation effects on magnetohydrodynamic couple stress nanofluid flow over a bidirectional stretching surface. Int. J. Heat Technol. **39**(1), 205–212 (2021)
16. Mahanthesh, B., Gireesha, B.J., Gorla, R.S.R., Makinde, O.D.: Magnetohydrodynamic three-dimensional flow of nanofluids with slip and thermal radiation over a

nonlinear stretching sheet: a numerical study. Neural Comput. Appl. **30**, 1557–1567 (2018)

17. Babu, M.J., Sandeep, N.: MHD non-Newtonian fluid flow over a slendering stretching sheet in the presence of cross-diffusion effects. Alex. Eng. J. **55**, 2193–2201 (2016)

18. Rashad, A.M.: Impact of thermal radiation on MHD slip flow of a ferrofluid over a non-isothermal wedge. J. Magn. Magn. Mater. **422**, 25–31 (2017)

19. Ellahi, R., Alamri, S.Z., Basit, A., Majeed, A.: Effects of MHD and slip on heat transfer boundary layer flow over a moving plate based on specific entropy generation. J. Taibah Univ. Sci. **12**(4), 476–482 (2018)

20. Das, M., Nandi, S., Kumbhakar, B., Seth, G.S.: Soret and Dufour effects on MHD nonlinear convective flow of tangent hyperbolic nanofluid over a bidirectional stretching sheet with multiple slips. J. Nanofluids **10**, 200–213 (2021)

21. Ullah, I., et al.: Theoretical analysis of activation energy effect on Prandtl-Eyring nanoliquid flow subject to melting condition. J. Non-Equilib. Thermodyn. **47**(1), 1–12 (2022)

22. Uddin, I., Ullah, I., Ali, R., Khan, I., Nisar, K.S.: Numerical analysis of nonlinear mixed convective MHD chemically reacting flow of prandtl-eyring nanofluids in the presence of activation energy and joule heating. J. Therm. Anal. Calorim. **145**, 495–505 (2021)

23. Khan, U., Zaib, A., Khan, I., Nisar, K.S.: Activation energy on MHD flow of titanium alloy (Ti6Al4V) nanoparticle along with a cross flow and streamwise direction with binary chemical reaction and non-linear radiation: dual solutions. J. Mater. Res. Technol. **9**(1), 188–199 (2020)

24. Fayyadh, M.M., Basavarajappa, M., Hashim, I., Mackolil, J., Nisar, K.S., Roslan, R., Allaw, D.: The mathematical model for heat transfer optimization of Carreau fluid conveying magnetized nanoparticles over a permeable surface with activation energy using response surface methodology. ZAMM **102**(11), e202100185 (2022)

25. Akbar, Y., Alotaibi, H., Iqbal, J., Nisar, K.S., Alharbi, K.A.M.: Thermodynamic analysis for bioconvection peristaltic transport of nanofluid with gyrotactic motile microorganisms and arrhenius activation energy. Case Stud. Therm. Eng. **34**, 102055 (2022)

26. Shoaib, M., Naz, S., Nisar, K.S., Raja, M.A.Z., Aslam, S., Ahmad, I.: MHD casson nanofluid in darcy-forchheimer porous medium in the presence of heat source and arrhenious activation energy: applications of neural networks. Int. J. Model. Simul. (2022). https://doi.org/10.1080/02286203.2022.2091973

27. Das, M., Kumbhakar, B., Singh, J.: Analysis of unsteady MHD Williamson nanofluid flow past a stretching sheet with nonlinear mixed convection, thermal radiation and velocity slips. J. Comput. Anal. Appl. **30**(1), 176–195 (2022)

28. Das, M., Kumbhakar, B.: Hall and ion slip effects on MHD bioconvective eyring-powell nanofluid flow past a slippery sheet under a porous medium considering Joule heating and activation energy. J. Porous Media **25**(5), 17–32 (2022)

29. Mustafa, M., Khan, J.A.: Numerical study of partial slip effects on MHD flow of nanofluids near a convectively heated stretchable rotating disk. J. Mol. Liq. **234**, 287–295 (2017)

30. Patel, H.R., Singh, R.: Thermophoresis, Brownian motion and non-linear thermal radiation effects on mixed convection MHD micropolar fluid flow due to nonlinear stretched sheet in porous medium with viscous dissipation, joule heating and convective boundary condition. Int. Commun. Heat Mass Transf. **107**, 68–92 (2019)

31. Kumar, K.A., Sugunamma, V., Sandeep, N.: Effect of thermal radiation on MHD casson fluid flow over an exponentially stretching curved sheet. J. Therm. Anal. Calorim. **140**, 2377–2385 (2020)
32. Das, M., Nandi, S., Kumbhakar, B.: Hall effect on unsteady MHD 3D Carreau nanofluid flow past a stretching sheet with Navier's slip and nonlinear thermal radiation. Palestine J. Math. 11(I), 95–108 (2022)
33. Mandal, S., Shit, G.C., Shaw, S., Makinde, O.D.: Entropy analysis of thermo-solutal stratification of nanofluid flow containing gyrotactic microorganisms over an inclined radiative stretching cylinder. Therm. Sci. Eng. Prog. **34**, 101379 (2022)
34. Bilal, M., Sagheer, M., Hussain, S.: Three dimensional MHD upper-convected Maxwell nanofluid flow with nonlinear radiative heat flux. Alex. Eng. J. **57**, 1917–1925 (2018)
35. Reddy, M.V., Lakshminarayana, P.: Cross-diffusion and heat source effects on a three-dimensional MHD flow of Maxwell nanofluid over a stretching surface with chemical reaction. Eur. Phys. J. Spec. Top. **230**(5), 1371–1379 (2021). https://doi.org/10.1140/epjs/s11734-021-00037-9
36. Sajid, M., Abbas, Z., Ali, N., Javed, T., Ahmad, I.: Slip flow of a maxwell fluid past a stretching sheet. Walailak J. Sci. Technol. **11**(12), 1093–1103 (2014)
37. Shehzad, S.A., Hayat, T., Alsaedi, A.: MHD flow of jeffrey nanofluid with convective boundary conditions. J. Braz. Soc. Mech. Sci. Eng. **37**, 873–883 (2015)
38. Khan, M.I., Waqas, M., Hayat, T., Khan, M.I., Alsaedi, A.: Chemically reactive flow of upper-convected Maxwell fluid with cattaneo christov heat flux model. J. Braz. Soc. Mech. Sci. Eng. **39**, 4571–4578 (2017)
39. Fatunmbi, E.O., Adeniyan, A.: Nonlinear thermal radiation and entropy generation on steady flow of magneto-micropolar fluid passing a stretchable sheet with variable properties. Results Eng. **6**, 100142 (2020)
40. Hayat, T., Awais, M.: Three-dimensional flow of upper-convected Maxwell (UCM) fluid. Int. J. Numer. Methods Fluids **66**, 875–884 (2011)